



Lanthanides based metal organic frameworks for luminescence sensing of toxic metal ions



Mahmoud Elcheikh Mahmoud^a, Zeinab Moussa^a, Thirumurugan Prakasam^b, Liang Li^b,
Mohamad G. Abiad^c, Digambara Patra^{a,*}, Mohamad Hmadeh^{a,**}

^a Chemistry Department, American University of Beirut, PO Box 11-0236, Riad El Solh, Beirut, 1107-2020, Lebanon

^b New York University Abu Dhabi (NYUAD), Experimental Research Building, Building C1, Saadiyat Island, Abu Dhabi, United Arab Emirates

^c Department of Nutrition and Food Sciences, American University of Beirut, PO Box 11-0236, Riad El Solh, Beirut, 1107-2020, Lebanon

ARTICLE INFO

Keywords:

Metal organic frameworks (MOFs)
Sensing
Fluorescence
Mercury
Heavy metals
Paraquat

ABSTRACT

Two set of lanthanides-based metal organic framework structures incorporating 2,6-naphthalenedicarboxylic acids and 1,5 dihydroxy-2,6-naphthalenedicarboxylic have been successfully synthesized and fully characterized. Interestingly, when 1,5 dihydroxy-2,6-naphthalenedicarboxylic was employed as organic linker, the hydroxyl groups were not involved in the coordination to the lanthanide clusters and therefore hydroxyl-functionalized lanthanides MOFs (AUBM-3) were obtained. The photophysical properties of both set of MOFs were studied and their sensing properties for toxic elements Pb(II), Cr(III), As(III), Cd(II), and Hg(II) and for paraquat were investigated. The hydroxyl-functionalized structures have shown to be promising luminescent sensory materials with high selectivity and sensitivity to mercury.

1. Introduction

Metal organic frameworks (MOFs), are a novel class of crystalline materials comprised of metal containing nodes, either a metal cation or metal clusters, and organic linkers connected via coordination bonds organized in a 3D network with uniform pore size [1,2]. MOFs have been an active area of research for the past two decades due to their rich chemistry and unique characteristics, including high surface area [3,4] which may exceed 10,000 m²/g, good mechanical and thermal stabilities [5,6], along with their possibility of being post-modified to target special applications [7]. MOFs offer great potential applications in several fields including catalysis [8–10], gas storage [11], magnetism [12,13], sensing, adsorption [14] and luminescence [15,16], production of metal nanoparticles [17], in addition to drug delivery [18], biomedical imaging [19], antimicrobial activity [20], dye sensitized solar cells [21], storage, encapsulation of dyes and polymer chains [22], also pH sensitive molecules [23,24]. Among these applications, sensing is one that has not been extensively investigated until recently. Consequently, available literature on such applications have reported the use of MOFs as sensors for explosives [25], chemical vapors [26], ions and small organic molecules [26]. Luminescent MOFs, particularly lanthanides MOFs (Ln-MOFs) can be considered one of the promising group of materials designed for

sensing. Ln-MOFs have distinctive luminescence properties, such as, high color purity, long-lived emission, great luminescence quantum yield, strident line emission and large stokes shift [27]. In addition to their emissive property, Ln-MOFs are characterized by their tuned coordination geometry, stability and magnetic properties [28]. These features qualify Ln-MOFs as efficient platform for sensing. For the development of an efficient and successful MOF sensor, both a binding site and a strong luminophore are required, thus, the importance of choosing a suitable ligand. When designing Ln-MOF, the organic linker is important for the structure, yet it can serve as antennae for the lanthanide ions [29]. Thereby, in agreement with the hard-soft acid base model, carboxylated ligands are a good option in building Ln-MOFs since the lanthanide ions are hard acceptors, thus, favoring the coordination with hard carboxylate groups [30]. The luminescence of the lanthanides can be enhanced and intensified upon choosing aromatic carboxylic groups, the latter being fine luminescent chromophores. Therefore, to obtain an effective Ln-MOF sensor, a promising approach is to select a conjugated aromatic organic linker with Lewis base sites, where the luminescence can be improved along with a potential metal ion binding site [19].

On the other hand, heavy metals are naturally occurring elements, and exist in varying concentrations in all ecosystems. Their density is greater than 5 g cm⁻³ [31]. Human activities (e.g. industrial processes, mining)

* Corresponding author.

** Corresponding author.

E-mail addresses: dp03@aub.edu.lb (D. Patra), mohamad.hmadeh@aub.edu.lb (M. Hmadeh).

<https://doi.org/10.1016/j.jssc.2019.121031>

Received 15 July 2019; Received in revised form 16 October 2019; Accepted 27 October 2019

Available online 2 November 2019

0022-4596/© 2019 Elsevier Inc. All rights reserved.

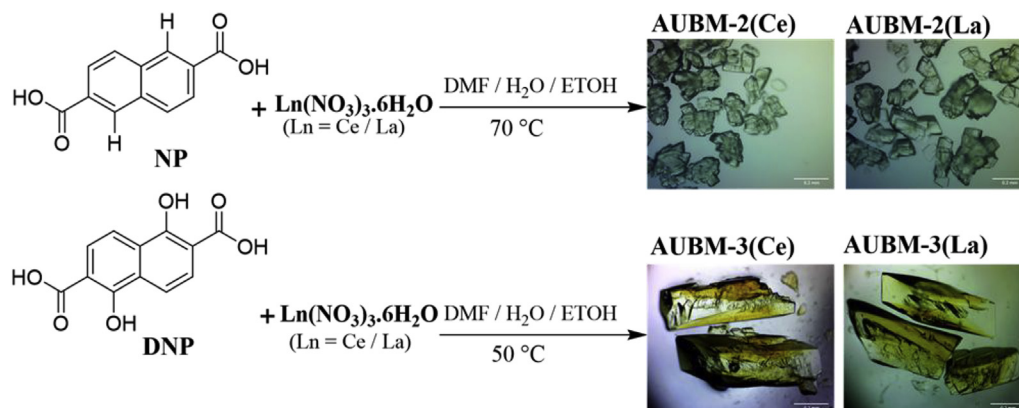
have drastically altered the biochemical cycles and balance of some heavy metals [32]. In low quantities, some heavy metals as iron, manganese, zinc and copper are nutritional necessities for a better life. On the other hand, heavy metals such as Cd, Pb, Cr, and Hg are poisonous and carcinogenic, even with trace amounts. Among various heavy metal ions, mercury is a very dangerous heavy metal that can induce many rigorous health problems such as damage to the nervous system and brain, kidney and the immune system [33]. Mercury exposure can provoke biochemical damage to tissues and genes via various mechanisms. It can interfere with the intracellular calcium homeostasis, alter membrane potential, disrupt protein synthesis, induce mitochondrial damage and cause lipid peroxidation [34]. With the mentioned risks that are related to mercury, a sensitive and selective detection of mercury can be considered as a priority. To detect mercury, several analytical techniques such as atomic absorption spectrometry [35], inductively coupled plasma atomic emission spectroscopy (ICP-AES) [36], gas chromatography-inductively coupled plasma-mass spectrometry [37], and atomic fluorescence spectroscopy (AFS) [38] are applied, however, these methods are often limited by the complex sample preparation, complicated devices and elevated cost [39]. Thus, it is of an importance to develop a non-demanding, sensitive and straightforward method for Hg^{2+} detection.

In this study, 2,6-naphthalenedicarboxylic acid (NP) and 1,5-dihydroxy-2,6-naphthalenedicarboxylic (DNP) (Scheme 1) were selected to react with lanthanides cations (La^{3+} and Ce^{3+}) to produce new lanthanides MOF structures. After varying many experimental conditions such as reagent concentrations, solvent mixtures, temperature and pHs, we succeeded in synthesizing four lanthanides MOFs using both linkers (NP and DNP). Herein, the synthesis, structural investigations, thermal stability, luminescent and sensing properties of the four MOFs namely AUBM-2 (Ce) and AUBM-2(La) for MOFs with NP and AUBM-3(Ce) and AUBM-3(La) for MOFs with DNP, were examined and reported. The two sets of MOFs (AUBM-2 and AUBM-3) exhibited different fluorescent properties that were greatly dependent upon the linker properties. The linker did not channel the energy to excite the lanthanide metals, thus, the fluorescence emission spectra didn't show the lanthanide metals bands. Having an iso-structural nature that was evident in their photophysical properties, Ce and La based MOFs were chosen to study their sensing behavior for different metal ions. Interestingly, AUBM-2 and AUBM-3 interacted with heavy metals and an intensive quenching of the AUBM-2 (Ce) luminescence in the presence of mercury was detected (K_{sv} value about $2000 M^{-1}$). This high quenching effect was only evident in the case of mercury, therefore, the Ce MOF can be considered as a sensitive and selective detector for mercury ions.

2. Experimental section

2.1. Materials and methods

All reagents and solvents employed were commercially available



Scheme 1. Synthesis scheme of AUBM-2 and AUBM-3.

from Sigma-Aldrich and SUGAI chemical industry and used without further purification. The Infrared (IR) spectra were recorded on a FT-IR spectrometer Thermo-Nicolet working in the transmittance mode, in the $450\text{--}3950\text{ cm}^{-1}$ range. Thermogravimetric Analysis (TGA) was performed with Netzsch TG 209 F1 Libra apparatus. Powder X-ray diffraction (PXRD) patterns were collected using a Bruker D8 advance X-ray diffractometer (Bruker AXS GmbH, Karlsruhe, Germany) at 40 kV, 40 mA (1600 W) using $Cu\ K\alpha$ radiation ($\lambda = 1.5418\text{ \AA}$). The absorption spectra were recorded at room temperature using JASCOV-570 UV-vis-NIR spectrophotometer. The steady state fluorescence measurements were recorded with resolution increment of 1 nm, slit 5 using a HORIBA Jobin Yvon Fluorolog-3 and the fluorescence program. The excitation source was 100 W xenon lamp, and the detector used was an R-928 operating at a voltage of 950 V. In order to regulate the temperature, a thermostat was coupled with the sample holder.

2.2. Synthesis of AUBM-2 and AUBM-3

Two novel Lanthanide MOFs were solvo-thermally synthesized by mixing 10 mg NP and 22 mg $Ln(NO_3)_3 \cdot 6H_2O$ ($Ln = La$ and Ce) in a mixed solvent system DMF/ H_2O /ETOH (10:1:1) at $70\text{ }^\circ\text{C}$ in a closed cap vial for 72 h, large crystals were obtained (yield 76% based on NP ligand). Taking the DNP organic linker as a starting material along with the same previously mentioned metal salts, additional two new lanthanide MOFs were prepared in the same solvent mixture in an open cap at 50 ° for 3 days (yield 80% based on DNP ligand). The single crystals obtained were insoluble in DMF and acetone. Elemental analysis: calculated (%): [AUBM-2(Ce)]; C 46.67; H 3.39; Ce 24.20; N 3.63; O 22.10; [AUBM-2(La)] C 46.77; H 3.40; La 24.04; N 3.64; O 22.15; found (%): [AUBM-2(Ce)]; C 46.98; H 3.32; Ce 24.05; N 3.41; O 22.83; [AUBM-2(La)] C 47.47; H 3.42; La 24.36; N 3.78; O 23.42. FT-IR (KBr, $\nu = 3500\text{--}500\text{ cm}^{-1}$): 3425(w), 1560(m), 1398(s), 1199(w), 1103(w), 800(m), 439(w). [AUBM-3(Ce)]; C 45.65; H 4.35; Ce 16.14; N 8.07; O 25.80; [AUBM-2(La)]; C 44.26; H 3.10; La 21.33; N 4.30; O 27.02; found (%): [AUBM-3(Ce)]; C 45.98; H 4.02; Ce 17.15; N 7.87; O 25.94; [AUBM-3(La)] C 45.25; H 3.31; La 22.14; N 4.13; O 26.42. FT-IR (KBr, $\nu = 3500\text{--}500\text{ cm}^{-1}$): 2939(w), 1597(m), 1413(s), 1272(s), 1191(m), 889(w), 793(s), 668(w), 432(w).

3. Results and discussion

3.1. Description of crystal structures

Analysis of X-ray diffraction data: Single X ray diffraction data collected from the single crystals obtained from the NP revealed that the two AUBM-2 are isostructural frameworks, these MOFs crystallize in a triclinic P-1 space group and cell parameters of ($a = 12.524(6)\text{ \AA}$, $b = 12.570(6)\text{ \AA}$, $c = 16.507(7)\text{ \AA}$; $\alpha = 81.716(9)\text{ }^\circ$, $\beta = 76.618(8)\text{ }^\circ$, $\gamma = 60.47(2)\text{ }^\circ$) with empirical formulas $C_{45}H_{39}Ce_2N_3O_{16}$ and $C_{45}H_{39}$

$\text{La}_2\text{N}_3\text{O}_{16}$ for AUBM-2(Ce) and AUBM-3(La) respectively. Each metal (Ce and La) is coordinated to 5 NP ligands and each of the ligands is coordinated to 2 metal centers to form an extended porous framework. The lanthanides cations are nine-coordinated to oxygen atoms to form a distorted monocapped square antiprism. The two adjacent metal centers are sharing one of the edges. In the coordination sphere, two of the 9 oxygens are from solvent molecules (DMF and water), the rest are five monodentate carboxylate groups, one chelating carboxylate group and one monodentate carboxylate group of NP ligand (Fig. 1). The M–O bond lengths and O–M–O bond angles for the coordination spheres are within the ranges of 2.381–2.659 Å and 68.35–147.6° respectively. (See supporting information for more details Tables S1–S4). The structure represent 1D pore channels with dimension of about $8 \times 10 \text{ \AA}^2$ which is defined by the distances of the binuclear unit viewed along z axis. Nevertheless, the solvent molecules coordinated to the lanthanides centre limit the accessibility to these pores. Finally, it can be seen that adjacent NP linkers represent π - π interactions with distances of around 3.6 Å (see Fig. 1).

To introduce new coordination units within the organic backbone and to decrease the number of coordinating solvent on the metal clusters, the DNP linker was employed for the MOF synthesis. This linker incorporates OH groups in ortho positions that could potentially participate in the coordination of the lanthanides and hence the chemical stability of the framework would be enhanced. Crystals with different shapes and colors were obtained for Ce and La. SXRD analysis of the two crystals showed 2 isostructural MOFs namely (AUBM-3) with the same topology but different from (AUBM-2). Interestingly, the OH groups in DNP, were not involved in the coordination of the Lanthanide cations. The obtained MOFs crystallize in a triclinic P-1 space group and cell parameters of ($a = 12.4869(15) \text{ \AA}$, $b = 12.5950(15) \text{ \AA}$, $c = 13.7583(17) \text{ \AA}$, $\alpha = 112.060(2)^\circ$, $\beta = 104.848(2)^\circ$, $\gamma = 102.417(2)^\circ$) with empirical formulas $\text{C}_{66}\text{H}_{75}\text{Ce}_2\text{N}_{10}\text{O}_{28}$ and $\text{C}_{24}\text{H}_{20}\text{LaN}_2\text{O}_{11}$ for AUBM-3(Ce) and AUBM-3(La) respectively. The cluster is composed of 2 cations that are coordinated to 6 ligands to form the network. The lanthanides cations are nine coordinated to O atoms to form monocapped square antiprism that are sharing one of the edges. 2 solvents molecules (DMF and water) are also involved in the coordination spheres of the cations, the remaining are from the DNP linkers. The M–O bond lengths and O–M–O bond angles for the coordination spheres are within the ranges of 2.46–2.57 Å and 51.168–145.6°. The structure of AUBM-3 represent an open framework with pore aperture of about $12 \times 23 \text{ \AA}^2$ which represents M-M distance across the diagonal of the pore along a direction (Fig. 1). Again,

these MOFs were stable in DMF and acetone but not in aqueous solution. Due to the low number of ligands coordinating to the metals, the thermal stability of this set of MOFs (AUBM-3) was even lower than the AUBM-2 as evidenced by the TGA plots recorded for these two MOFs. The hydroxyl groups are free and not involved in the coordination of lanthanide which leave them available to interact with guest molecules and ions (see Fig. 1 and Fig. S1). In order to assess this porosity, the N_2 isotherm was performed on the activated for AUBM-2(Ce) and AUBM-3(Ce) and the Brunauer–Emmett–Teller (BET) surface area was determined to be $82 \text{ m}^2/\text{g}$ and $190 \text{ m}^2/\text{g}$ respectively (Fig. S2).

3.2. Powder X-ray diffraction and thermal gravimetric analyses

To verify the phase purity of the newly synthesized MOFs, the powder X-ray diffraction (PXRD) patterns were recorded and compared to the simulated patterns. As shown in Fig. S3 the diffraction peaks of the as-synthesized AUBM-2 and AUBM-3 are in agreement with the simulated data confirming the phase purity of the MOFs.

Thermal gravimetric analyses (TGA) of both series of lanthanide MOFs were carried between 30 and 1000 °C. The thermal profiles corresponding to AUBM-3(Ce) and AUBM-3(La) were analogous due to the isostructural character. A weight loss of 10% was obtained in the range of 77–140 °C corresponding to the loss of DMF molecules. The major mass loss of 30% occurred at 200 °C and is attributed to the decomposition of the organic framework and the discharge of the organic linker. The remaining residues are mainly the corresponding metal oxides. Similarly, the weight loss of AUBM-2 of both Ce and La-MOF was alike as a result of the isostructural nature. Compared to AUBM-3 MOFs this set showed a better thermal stability with the major weight loss (35%) corresponding to the burning of the framework occurred at 552 °C. Between 111 and 200 °C there is a 20% weight loss that is linked to the loss of the coordinated DMF molecules. The final residues are that of respective metal oxides Fig. S4.

3.3. FTIR spectral analysis

The FTIR spectrum of the synthesized AUBM-2 is shown in Fig. S5A. The spectrum indicates an up-field shift in the carbonyl stretches 1682, 1659, 1650 and 1661 cm^{-1} for AUBM-2(La) and AUBM-2(Ce). Regarding AUBM-3, the two C=O groups for the ligand displays an up-field shifts from 1599 and 1656 to 1596 and 1653 cm^{-1} respectively for AUBM-3(La). Similar up-field shifts were observed for AUBM-3(Ce).

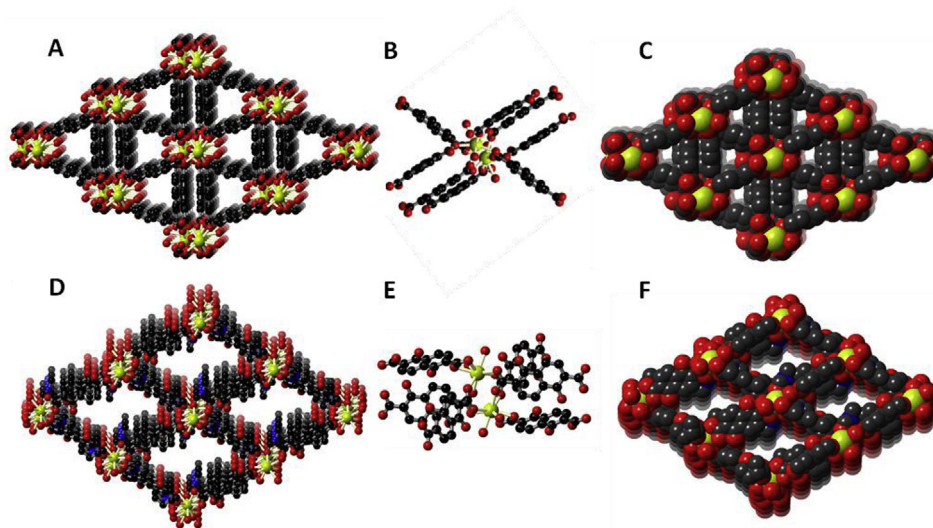


Fig. 1. Crystal structures of AUBM-2(Ce) (A), coordination mode in the cluster of AUBM-2 (B), space filling representation of AUBM-2 (C). Crystal structure of AUBM-3(Ce) (D), The coordination mode in AUBM-3 (E), space filling representation of AUBM-3 (F). Where Ce: yellow, O: red, N: blue, C: grey. (For interpretation of the references to color in this figure legend, the reader is referred to the Web version of this article.)

The characteristic broad band of the hydroxyl group within the solids were detected between 3200 and 3550 cm^{-1} designating the retention of the free OH groups as shown in Fig. S5B.

3.4. Photophysical properties

Luminescence in MOFs is usually dependent on the building components: the organic linker mainly conjugated one, metal ions or cluster and in few cases a result of adsorbed guest molecules that include to the emission. Organic linkers characterized by a rigid molecular backbone along with aromatic parts or extended π systems are commonly used in building MOFs. Luminescence generated mainly by the π electrons of the organic linker can be either linker based fluorescence or ligand-to-ligand charge transfer (LLCT) [28]. The photophysical properties of the linker are affected by the later arrangement in the framework thus resulting in different photoemission compared to that of the free form. In lanthanide MOFs, metal centered luminescence is dominant when an efficient intersystem crossing occurs between the organic linker and the metal. Linkers that allow the delivery of the excitation energy from their triplet excited states to the emissive states of the lanthanides result in the metal sensitization and the characteristic emission of the lanthanide metal is observed [28]. The photophysical properties of the synthesized MOFs and their linkers were investigated using UV-visible and fluorescence spectroscopy.

3.4.1. UV-vis spectroscopic measurements

The MOF crystals were washed and sonicated with DMF to have a homogeneous suspension and absorbance spectra were measured at room temperature. The isostructural property of AUBM-3 was reflected in the UV absorbance. In Fig. S6B, the absorbance spectrum of the organic linker shows an absorbance maximum at 346 nm in addition to another absorption peak at 296 nm. This is similar to one expects for NP linker. However, AUBM-2 shows an absorption maximum at 294 nm and a relatively weak absorption band at 420 nm. The changes in the absorption spectrum of the linker can be linked to the coordination between the organic linker and the metal ion in the framework. As for the DNP linker, the maximum absorbance is observed at 370 nm, with two other minor peaks similar to that of the NP linker at 314 and 297 nm. This red shift in the absorption spectrum of the DNP linker is a result of the presence of the hydroxyl groups which may further boost the conjugation in the parent ligand molecule and possibly form hydrogen bond with solvent molecules. The absorption spectra of AUBM-3 were similar with two maxima recorded at 399 nm and 300 nm along with shoulder bands at 370–380 nm Fig. S6A. This further shift in the absorption spectra is induced by the linker interaction in the organic framework. A deeper study of the absorption spectra of the linkers along with the MOFs where

the metal ions was cerium or lanthanum was performed. The UV-visible spectra were measured at different concentrations of the latter species Fig. S7 (A and B). Furthermore, it is clear from the figures that there was no change in the shape of the spectrum of both MOFs and the linkers at varying concentrations.

3.4.2. Fluorescence spectroscopic study

The washed MOFs and the dissolved linkers were excited at several wavelengths and the fluorescence spectra were measured at various concentrations in DMF at 298 K. As presented in Figs. S8A and S9A, at first the DNP linker alone was excited at three different wavelengths, such as at 300, 370 and 400 nm at various concentrations. When excited at 370 and 400 nm, there is a significant red shift in the emission spectra from 436 nm to 500 nm along with a change in the shape of the emission spectra upon increasing the concentration of the linker. When excited at 300 nm, at higher concentration there is less red shift than the previously noted with the emission maximum shifting from 436 to 460 nm. This change at higher concentration is most likely caused by the formation of dimmers or aggregates of the linkers. A similar outcome is also found for the NP linker with a red shift from 377 nm to 400 nm when excited at 300 nm given in Fig. S8. Those changes that are also observed when excited at 370 nm and 400 nm are a result of the aggregation free linker molecules at higher concentration.

The MOF crystals were diluted in DMF and the fluorescence spectra were measured at three different excitation wavelengths with varying concentrations of the MOFs in DMF. As shown in Figs. S8C and S9C, when excited at 300 nm, AUBM-3(Ce) gave a maximum fluorescence intensity centered at 436 nm, with another emission peak at 358 nm. Upon an excitation at 370 nm and 400 nm, AUBM-3(Ce) showed close emission spectra with the maximum emission occurring in both excitation conditions around 438 nm. Similar results were obtained for AUBM-3(La) Figs. S8D and S9D thus, it can be concluded that the lanthanide metal doesn't affect the emission properties, at least the photophysical behavior of the MOFs. However, when compared to the free linker, at high concentrations the new species emitting at higher concentrations is no longer evident when the linker is incorporated within the framework. Thus, the interaction between the metal and the linker hinders the interaction between the organic linker themselves. Moreover, when excited at 300 nm, the linker does not show a peak at 358 nm thus this outcome in the MOFs is an impact of the new arrangements and interactions the organic linker undergoes within the MOF. The fluorescence spectrum of AUBM-2(Ce) exhibited a maximum emission at 375 nm when excited at 300 nm (Figs. S8 and S9). When excited at 370 nm, this emission shifted to 415 nm. This suggests that there are two chromophores, which absorb and emit in two different wavelength regions. One of them primarily absorbs ~290–300 nm and emits at ~350–370 nm

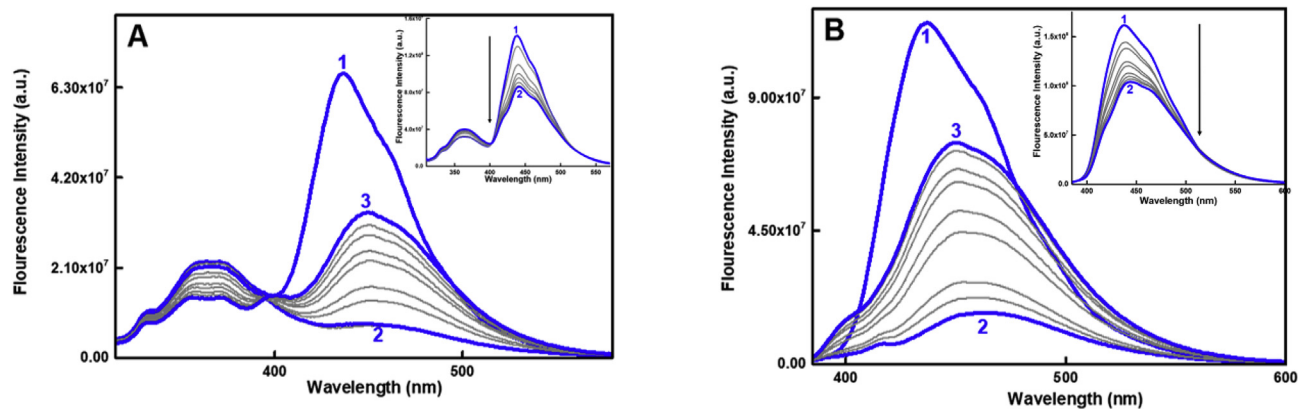


Fig. 2. Fluorescence spectra of the AUBM-3(Ce) excited at 300 nm (A) and 370 nm (B) in the presence of lead ions, where (1) $[\text{Pb}^{2+}] = 0.00 \mu\text{M}$, (2) $[\text{Pb}^{2+}] = 0.014 \mu\text{M}$, and (3) $[\text{Pb}^{2+}] = 0.189 \mu\text{M}$. Inset (A) and (B) fluorescence spectra of AUBM-3(Ce) at 300 nm, 370 nm respectively Where (1) $[\text{Pb}^{2+}] = 0.00 \mu\text{M}$, (2) $[\text{Pb}^{2+}] = 0.009 \mu\text{M}$.

whereas the other species absorbs at $\sim 360\text{--}400$ nm and emits at $\sim 400\text{--}450$ nm. However, there is also possibility of energy transfer such as FRET from species one to two, which influence the fluorescence spectral behavior [40].

3.5. Metal sensing

To study the ability of the synthesized lanthanides MOFs (AUBM-2 and AUBM-3) to detect and sense heavy metal ions, the MOFs were suspended in DMF and the heavy metal ion solution prepared in DMF were added in increasing concentrations to the MOF sample. The sensing potentials of the lanthanide's MOFs were tested with five ions (e.g. lead, cadmium, arsenic, mercury and chromium). From each set, samples were excited at two different wavelengths, 300 and 370 nm aiming to target two different fluorescent species present in MOFs. The outcome did not differ when the metal (La or Ce) was changed, thus, the interaction and sensing using cerium will only be reported and discussed here.

3.5.1. Interaction of lead ions with AUBM-2(Ce) and AUBM-3(Ce)

Fig. S10A and 2A show fluorescence spectra of AUBM-2(Ce) and AUBM-3(Ce) respectively, with increasing concentrations of lead ion upon exciting at 300 nm. For the AUBM-2(Ce), with increasing concentrations of the Pb^{2+} ion, there is an increase in the fluorescence intensity at 374 nm, whereas in case of AUBM-3(Ce) addition of 5 μL of the Pb ion stock (8.3 μM) red shifted the emission maximum from 436 nm (in the

absence of Pb^{2+}) to 452 nm with seven folds decrease in the fluorescence intensity Fig. 2A. As it can be seen in the inset of Fig. 2A, this quenching was monitored gradually by using a 5 times diluted stock solution of Pb ions. Further increase in Pb^{2+} concentration increased the fluorescence intensity centered at 452 nm. Nevertheless, the overall fluorescence intensity at 452 nm was still less than that in the absence of Pb^{2+} ion. This observation could be due to the fact that binding of Pb^{2+} ion with hydroxyl group of the linker forms a completely new complex with an emission peak at 452 nm and the population of this complex increased with increase in concentration of Pb^{2+} ion in solution, thus, boosting fluorescence intensity at 452 nm. This indicates that at low concentration of Pb^{2+} ion (below 0.014 μM), a quenching of the fluorescence peak at 452 was observed, however, at higher Pb^{2+} concentrations, an enhancement of the MOF fluorescence centered at the same peak was obtained.

A minor emission peak at 365 nm is also relevant at 300 nm excitation for AUBM-3(Ce), which was quenched with lead concentration. The quenching rate was calculated from the Stern Volmer plot with a Ksv value of 747 M^{-1} Fig. S11. This quenching was absent in the AUBM-2(Ce). When excited at 370 nm, as shown in Fig. S10B, the fluorescence of AUBM-2(Ce) at 436 nm decreased with increasing concentration of lead ions. Similarly, for AUBM-3(Ce), the increase in the lead concentrations quenched the fluorescence emission at 451 nm along with a red shift in the emission maximum, which was identical to that obtained at 300 nm excitation. Similar data were obtained for the AUBM-3(La)

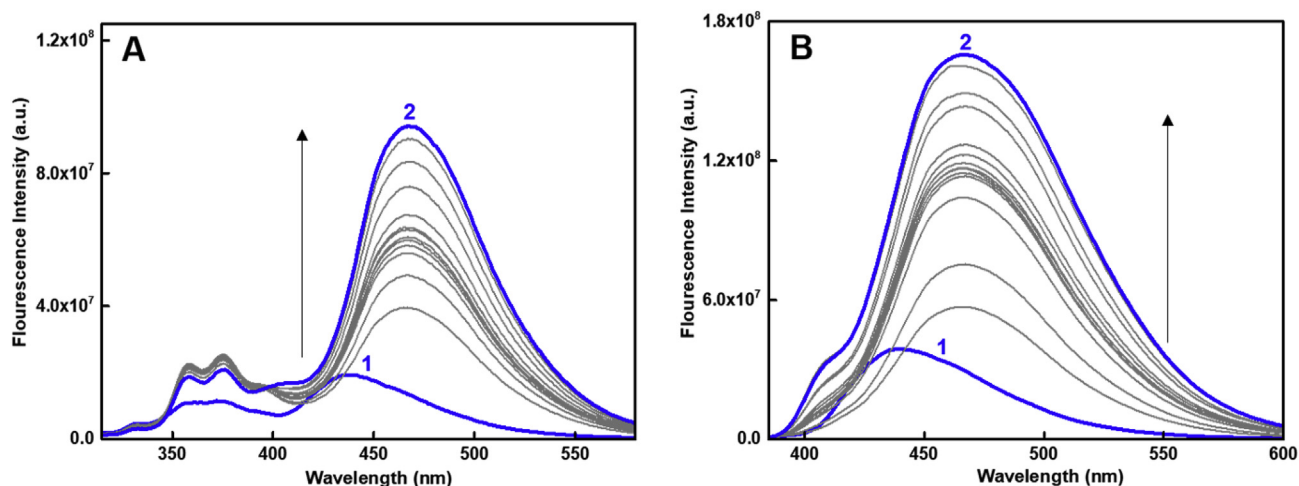


Fig. 3. Fluorescence spectra of the AUBM-3(Ce) excited at 300 nm (A) and 370 nm, (B) in the presence of chromium, where (1) $[\text{Cr}^{3+}] = 0.00 \mu\text{M}$, (2) $[\text{Cr}^{3+}] = 0.215 \mu\text{M}$.

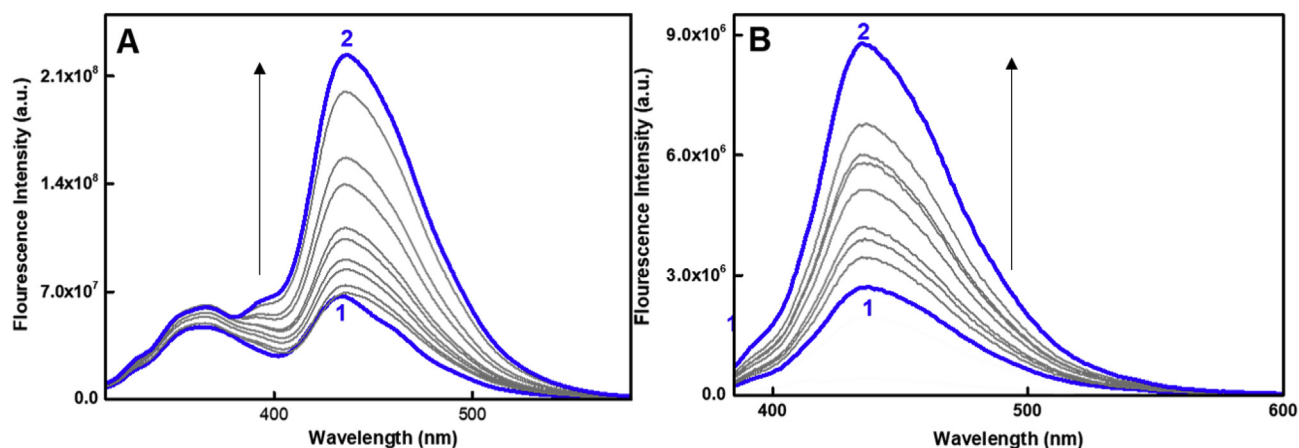


Fig. 4. Fluorescence spectra of the AUBM-2(Ce) excited at 300 nm (A) and 370 nm (B) in the presence of arsenic ions, where (1) $[\text{As}^{3+}] = 0.00 \mu\text{M}$, (2) $[\text{As}^{3+}] = 0.123 \mu\text{M}$.

when excited at 300 nm, with a higher Ksv value 908 M^{-1} . Thus, the best approach to estimate the presence of lead would be to monitor the emission at 365 nm for the AUBM-3(Ce) excited at 300 nm.

3.5.2. Interaction of chromium ions with AUBM-2(Ce) and AUBM-3(Ce)

As shown in Fig. S12 (A and B), interaction between AUBM-2(Ce) with increasing concentration of chromium ion resulted in an enhancement in fluorescence intensity while exciting at 300 nm or 370 nm. However, the emission maximum was affected to a small extent in the presence of the chromium ions and the emission was more sensitive to the chromium ions at 300 nm excitation than that induced when excited

at 370 nm. In the case of AUBM-3(Ce) (see Fig. 3), enhancement of fluorescence intensity was also observed with increasing concentrations of the chromium ions except that a 30 nm red shift in the emission maximum (from 437 to 467) was observed. Similar results were obtained at 370 nm. This indicates chromium may not specifically bind the hydroxyl group of the ligand rather it gets buried/adsorbed on the MOFs which influence the fluorescence properties of MOFs.

3.5.3. Interaction of arsenic and cadmium ions with AUBM-2(Ce) and AUBM-3(Ce)

AUBM-2(Ce) and AUBM-3(Ce) were excited at 300 nm and 370 nm in

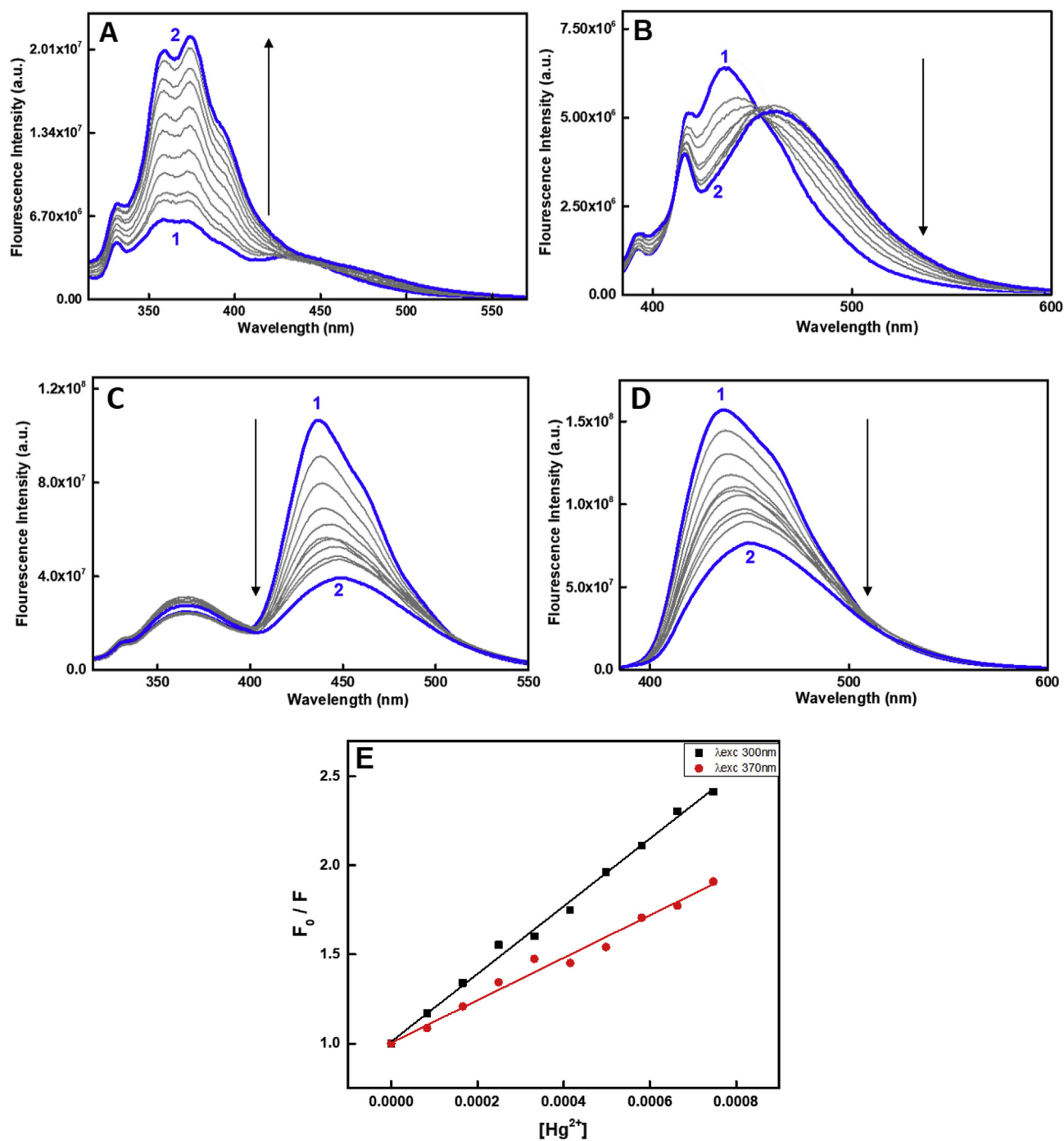


Fig. 5. Fluorescence spectra of the AUBM-2(Ce) excited at 300 nm (A) and 370 nm (B) in the presence of mercury ions in addition to the spectra obtained for AUBM-3(Ce) under same condition upon exciting at 300 nm (C) and 370 nm (D). Stern-volmer Plots for AUBM-3(Ce) in the presence of mercury ions (E), where (1) $[\text{Hg}^{2+}] = 0.00 \mu\text{M}$, (2) $[\text{Hg}^{2+}] = 0.136 \mu\text{M}$.

the presence of increasing concentrations of metal ions (arsenic and cadmium). As shown in Fig. 4 and S13, the increase in the concentration of the arsenic ion resulted in mild enhancement in the fluorescence emission without any changes or shifts in the spectrum as in the case of the previously discussed metals. Similar results were also obtained with cadmium (Fig. S14). Indeed, the strongest enhancement after the addition of Cd ions to a total concentration of 830 μM by a factor of 21 was observed for AUBM-2(Ce) when excited at 370 nm compared to a 1.5-fold of enhancement when excited at 300 nm. The fluorescence was enhanced by 3 times when AUBM-3(Ce) was excited at 300 nm and about 2-fold increase in the emission when AUBM-3(Ce) was excited at 370 nm (Fig. S14).

3.5.4. Interaction of mercury ions with AUBM-2(Ce) and AUBM-3(Ce)

The interaction between the cerium-based MOFs and the mercury metal ions was the most interesting data among the five heavy metals. When excited at 300 nm in the presence of increasing concentrations of Hg ions, the emission intensity of the AUBM-2(Ce) at 375 nm was enhanced. However, when excited at 370 nm under the same conditions, the Hg ions induced a quenching effect with a gradual red shift in the emission spectra (~ 30 nm red shift) with increasing concentrations of mercury. In the case of AUBM-3(Ce), the fluorescence emission after excitation at 300 nm was quenched with a small red shift of the emission maximum at higher concentration of mercury ions (Fig. 5). The corresponding Ksv value obtained from the Stern-volmer plot was remarkable, $\sim 1899.6 \text{ M}^{-1}$. Contrary to its behavior in the presence of lead, the emission intensity at 364 nm was enhanced. When excited at 370 nm, the maximum emission at 436 nm was quenched in addition to a red shift of 14 nm in the emission maximum. The Ksv value was estimated as 1192.6 M^{-1} less than that was found when exciting at 300 nm. This quenching is linked to the hydroxyl groups of the DNP. As shown from the single XRD data, the OH groups are not involved in the coordination the lanthanide clusters of AUBM-3 thus providing an interaction site with metals. The recyclability of AUBM-3(Ce) was investigated by washing the resulting MOF with acetone several times. Interestingly, the recovered MOF crystals were efficiently used to detect and sense mercury ions with no obvious change in the fluorescence spectrum (Fig. S15). Also, the regeneration of the crystals doesn't affect the crystallinity of the MOF structure as evidenced in the PXRD pattern (Fig. S16).

Based on the reported experimental data, the newly fluorescent synthesized MOFs showed interaction with heavy metals however, it showed selective quenching for Hg at 436 nm after excitation at 300 nm and selective quenching in the case of the lead metal ions in the 365 nm emission after excitation at 300 nm. Similarly, the fluorescence of AUBM-3(Ce) at 370 nm excitation was quenched only in the case of mercury ions. The quenching effect induced by the mercury metals was appreciable with Ksv values of 1899.6 and 1192.6 M^{-1} after exciting at 300 nm and 370 nm respectively, a table of comparison of different luminescent MOFs for detecting Hg(II) is given in the SI (Table S5). And shows that the detection limit of Hg and the calculated Ksv are within the range of the best reported MOF structures. Thus, we can say that the AUBM-3(Ce) can be used as a selective sensor for mercury among 5 common heavy metals. The selectivity towards metal ions of four different kinds of MOFs under investigation is summarized in Fig. 6.

Two different trends were observed during luminescent titrations. As found in the UV-visible absorption and fluorescence spectra, both the MOFs (AUBM-2 and AUBM-3) have two absorbing/emitting species depending on the excitation wavelengths (300 or 370 nm). In literature where MOFs were employed in metal sensing applications [41], several explanations regarding their luminescence behavior (quenching or enhancement) have been investigated such as: (i) the ion exchange between the guest ions and the metal ions of the MOF clusters [42,43], (ii) the resonance energy transfer [44], (iii) the collapse of the framework upon addition of the metal ions [45] and (iv) the weak interactions between guest metal ions and the functional group within the organic linkers of the MOFs [46]. In order to understand the mechanism behind

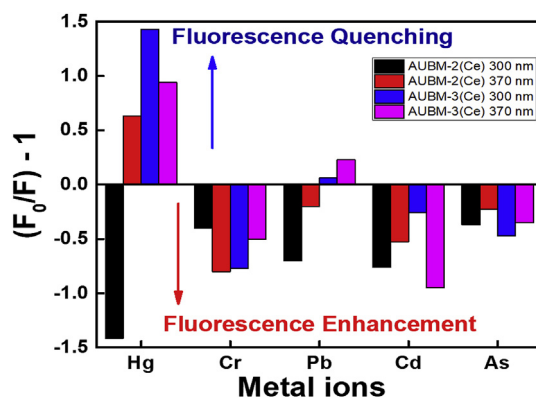
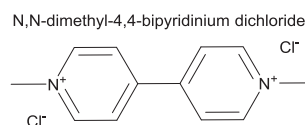


Fig. 6. Influence of fluorescence change of different MOFs in the presence of various metal ions during optical sensing. The concentrations of metal ions were fixed at 8.33 mM. F_0 and F are the fluorescence intensity in the absence and presence of metal ion, respectively.

the spectral changes observed throughout the sensing studies in the present case, several experiments were performed. The PXRD patterns of the MOFs after sensing were recorded and showed that the crystallinity of the frameworks was not affected (Fig. S16), which exclude the collapse of the framework upon addition of the cations. Furthermore, no Pb, As, Cd or Hg was observed in the SEM-EDX analysis performed on the MOFs crystals after sensing (Fig. S17). Finally, UV-vis absorption spectra for the metal ions and AUBM-3(Ce) were recorded, a spectral overlap between the absorption spectrum of Hg^{2+} solution and the absorption peaks of AUBM-3(Ce) was observed (Fig. S20) while other metal ion solutions do not. This overlapping suggests that the fluorescence quenching by Hg^{2+} ion may be attributed to the absorption competition at the excitation wavelength (300 and 370 nm) between Hg^{2+} solution and AUBM-3(Ce). Moreover, as shown from the single XRD data, the OH groups are not involved in the coordination of the lanthanide clusters of AUBM-3 which provides an interaction site for the metal ions during sensing. A significant red shift (30 nm) was observed by increasing Hg^{2+} concentration for AUBM-2(Ce) at 370 nm, which may be caused by the solvatochromism effect [47] suggesting a more polar environment for the chromophore in the presence of Hg^{2+} . This can be possible only when some exposed free carboxylate units from the organic linkers resulted from the defects in the crystals (a very common phenomenon in MOFs structures) or free OH group could be involved in the weak interactions with the studied cations. Such adsorption enhances the fluorescence of the MOFs, as observed for AUBM-2(Ce) at 300 nm and other metal ions.

3.6. Paraquat sensing



Paraquat (Methyl viologen, MV) is a poisonous bipyridinium compound used as contact herbicide. Paraquat binds strongly to soil particles and tends to remain strongly bound for a long time in an inactive state, although it can also desorb again and become biologically active. Half-life in soil can be up to 20 years. Therefore, developing a sensing technique for such compound is particularly interesting. Since our AUBM-2 and AUBM-3 incorporate Naphthalene based linkers which are known to be electron rich species, we believe that these MOFs could interact with electron acceptor units such as viologen. Indeed, charge transfer (CT) complexes have been reported based on the interaction between DNP or NP units and MV^{2+} [48]. Interestingly, the fluorescence of AUBM-2(La) and AUBM-2(Ce) were completely quenched (see Fig. 7)

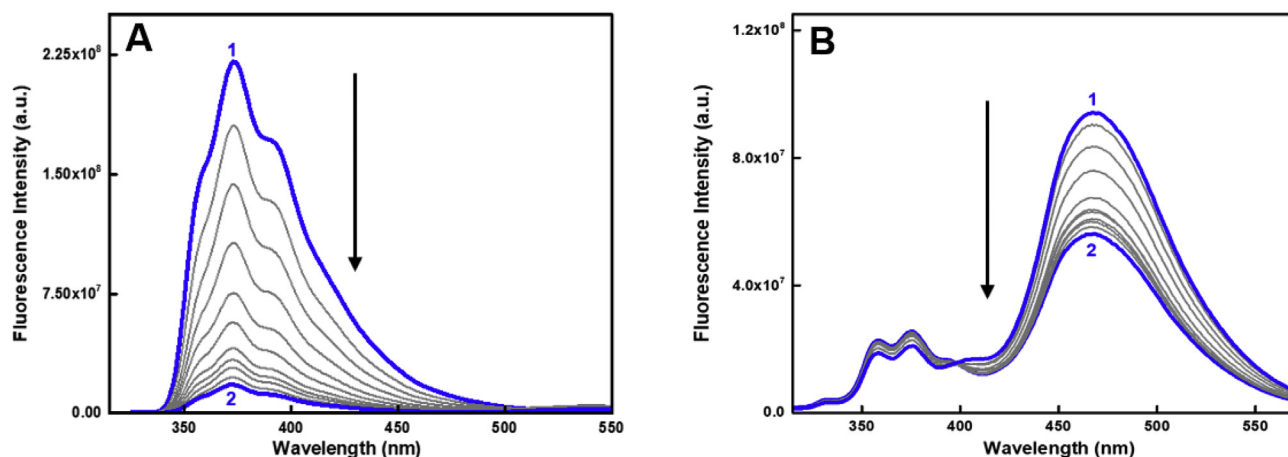


Fig. 7. Fluorescence spectra of the AUBM-2(La) (A) and AUBM-2(Ce) (B) excited at 300 nm, where (1) $[MV^{2+}] = 0.0$ mg/mL and (2) $[MV^{2+}] = 50$ mg/mL at ambient temperature.

upon addition of MV^{2+} with K_{sv} values $21 M^{-1}$ and $9 M^{-1}$ respectively. Especially, AUBM-2 (La) fluorescence was remarkably quenched as shown in Fig. 7A. It can be noted that initially till 80 mM of MV^{2+} , the quenching rate for F_0/F of AUBM-3(La) vs. $[MV^{2+}]$ was linear as given in inset of Fig. S18 and it obeys Stern-Volmer equation with a K_{sv} value $\sim 21 M^{-1}$. However, as the concentration increased, the trend showed an upward curvature. Since AUBM-2(La) can form charge transfer complex with MV^{2+} , it is expected that initially the quenching rate follows a dynamic quenching mechanism till ~ 20 mM and afterwards at higher concentration of MV^{2+} both static and dynamic quenching mechanisms are operative giving an upward curvature in the Stern-Volmer plot. It was found that this quenching trend of AUBM-2(La) by MV^{2+} continued till up to 50 mg/mL, thus, it can be useful for the determination of MV^{2+} in environmental samples.

4. Conclusion

Four highly luminescent lanthanides-based metal-organic frameworks were successfully synthesized using solvothermal processes. All the four lanthanides-based MOFs were thoroughly characterized using single crystal and powder X-ray diffraction, TGA, IR, UV-Vis, fluorescence studies. The luminescent properties of the all four MOFs were explored and their ability for heavy metal sensing such as Pb (II), Cr (III), As (III), Cd (II) and Hg (II) and paraquat were tested in solution. Among the tested MOFs, cerium-based MOF (AUBM-3(Ce)) was found to be highly selective for mercury sensing in solution. Highly selective and stable luminescent lanthanides design and synthesis using our current knowledge for selective detection of heavy metal in aqueous solution is underway in our laboratory.

The structural information of AUBM-2(La), AUBM-2(Ce), AUBM-3(La) and AUBM-3(Ce) are available free of charge from the Cambridge Crystallographic Data Centre under the reference numbers: CCDC 1,841,240, CCDC 1,841,235, CCDC 1,841,198 and CCDC 1,841,199, respectively.

Declaration of competing interest

The authors declare that they have no known competing financial interests or personal relationships that could have appeared to influence the work reported in this paper.

Acknowledgment

This research work was funded by the American University of Beirut (AUB) University Research Board (URB) and the Lebanese National

Council for Scientific Research (#103496 and #103487) and the Masri Institute (#103214). The authors would like to thank the personnel at the Kamal A. Shair Central Research Science Laboratory (CRSL) for their support and assistance. T.P. and L.L. thank NYUAD for its generous support for the research program at NYUAD and the authors also thank the Core Technology Platforms at NYUAD.

Appendix A. Supplementary data

Supplementary data to this article can be found online at <https://doi.org/10.1016/j.jssc.2019.121031>.

References

- [1] S. Yuan, L. Feng, K. Wang, J. Pang, M. Bosch, C. Lollar, Y. Sun, J. Qin, X. Yang, P. Zhang, Q. Wang, L. Zou, Y. Zhang, L. Zhang, Y. Fang, J. Li, H.-C. Zhou, *Adv. Mater.* 30 (2018) 1704303.
- [2] Q.-G. Zhai, X. Bu, X. Zhao, D.-S. Li, P. Feng, *Acc. Chem. Res.* 50 (2017) 407–417.
- [3] H. Furukawa, K.E. Cordova, M. O’Keeffe, O.M. Yaghi, *Science* 341 (2013) 1230444.
- [4] D. Saliba, M. Ammar, M. Rammal, M. Al-Ghoul, M. Hmadeh, *J. Am. Chem. Soc.* 140 (2018) 1812–1823.
- [5] H. Wu, T. Yildirim, W. Zhou, *J. Phys. Chem. Lett.* 4 (2013) 925–930.
- [6] K.S. Park, Z. Ni, A.P. Côté, J.Y. Choi, R. Huang, F.J. Uribe-Romo, H.K. Chae, M. O’Keeffe, O.M. Yaghi, *Proc. Natl. Acad. Sci. U.S.A.* 103 (2006) 10186–10191.
- [7] K.K. Tanabe, S.M. Cohen, *Chem. Soc. Rev.* 40 (2011) 498–519.
- [8] S. Horike, M. Dincă, K. Tamaki, J.R. Long, *J. Am. Chem. Soc.* 130 (2008) 5854–5855.
- [9] D.-S. Liu, Z.-J. Qiu, X. Fu, Y.-Z. Liu, P. Ding, Y.-X. Zhu, Y. Sui, *J. Solid State Chem.* 278 (2019) 120879.
- [10] D.-S. Liu, Y. Sui, G.-M. Ye, H.-y. Wang, J.-Q. Liu, W.-T. Chen, *J. Solid State Chem.* 263 (2018) 182–189.
- [11] R. Matsuda, R. Kitaura, S. Kitagawa, Y. Kubota, R.V. Belosludov, T.C. Kobayashi, H. Sakamoto, T. Chiba, M. Takata, Y. Kawazoe, Y. Mita, *Nature* 436 (2005) 238–241.
- [12] P. Dechambenoit, J.R. Long, *Chem. Soc. Rev.* 40 (2011) 3249–3265.
- [13] W.-W. Xiong, E.U. Athresh, Y.T. Ng, J. Ding, T. Wu, Q. Zhang, *J. Am. Chem. Soc.* 135 (2013) 1256–1259.
- [14] H. Atallah, M. Elcheikh Mahmoud, A. Jelle, A. Lough, M. Hmadeh, *Dalton Trans.* 47 (2018) 799–806.
- [15] H.R. Moon, D.-W. Lim, M.P. Suh, *Chem. Soc. Rev.* 42 (2013) 1807–1824.
- [16] D.-S. Liu, Y. Sui, W.-T. Chen, P. Feng, *Cryst. Growth Des.* 15 (2015) 4020–4025.
- [17] P. Horcajada, R. Gref, T. Baati, P.K. Allan, G. Maurin, P. Couvreur, G. Férey, R.E. Morris, C. Serre, *Chem. Rev.* 112 (2012) 1232–1268.
- [18] S. Keskin, S. Kizilel, *Ind. Eng. Chem. Res.* 50 (2011) 1799–1812.
- [19] H. Deng, S. Grunder, K.E. Cordova, C. Valente, H. Furukawa, M. Hmadeh, F. Gándara, A.C. Whalley, Z. Liu, S. Asahina, H. Kazumori, M. O’Keeffe, O. Terasaki, J.F. Stoddart, O.M. Yaghi, *Science* 336 (2012) 1018–1023.
- [20] B. Mortada, T.A. Matar, A. Sakaya, H. Atallah, Z. Kara Ali, P. Karam, M. Hmadeh, *Inorg. Chem.* 56 (2017) 4739–4744.
- [21] V. Nevruzoglu, S. Demir, G. Karaca, M. Tomakin, N. Bilgin, F. Yilmaz, *J. Mater. Chem.* 4 (2016) 7930–7935.
- [22] W.-W. Xiong, J. Miao, K. Ye, Y. Wang, B. Liu, Q. Zhang, *Angew. Chem. Int. Ed.* 54 (2015) 546–550.
- [23] Z. Moussa, M. Hmadeh, M.G. Abiad, O.H. Dib, D. Patra, *Food Chem.* 212 (2016) 485–494.

- [24] S.S. Nagarkar, B. Joarder, A.K. Chaudhari, S. Mukherjee, S.K. Ghosh, *Angew. Chem. Int. Ed.* 52 (2013) 2881–2885.
- [25] Z. Xie, L. Ma, K.E. deKrafft, A. Jin, W. Lin, *J. Am. Chem. Soc.* 132 (2010) 922–923.
- [26] P. Deria, J.E. Mondloch, O. Karagiari, W. Bury, J.T. Hupp, O.K. Farha, *Chem. Soc. Rev.* 43 (2014) 5896–5912.
- [27] B.V. Harbuzaru, A. Corma, F. Rey, P. Atienzar, J.L. Jordá, H. García, D. Ananias, L.D. Carlos, J. Rocha, *Angew. Chem. Int. Ed.* 47 (2008) 1080–1083.
- [28] H. Zhang, L. Zhou, J. Wei, Z. Li, P. Lin, S. Du, *J. Mater. Chem.* 22 (2012) 21210–21217.
- [29] J.-M. Zhou, W. Shi, N. Xu, P. Cheng, *Inorg. Chem.* 52 (2013) 8082–8090.
- [30] S.J. Hawkes, *J. Chem. Educ.* 74 (1997) 1374.
- [31] L. Pari, P. Murugavel, S.L. Sitasawad, K.S. Kumar, *Life Sci.* 80 (2007) 650–658.
- [32] K. Jomova, M. Valko, *Toxicology* 283 (2011) 65–87.
- [33] F. Zahir, S.J. Rizwi, S.K. Haq, R.H. Khan, *Environ. Toxicol. Pharmacol.* 20 (2005) 351–360.
- [34] L. Patrick, *Mercury Toxicity and Antioxidants: Part I: Role of Glutathione and Alpha-Lipoic Acid in the Treatment of Mercury Toxicity*, 2003.
- [35] H.N. Chou, C.A. Naleway, *Anal. Chem.* 56 (1984) 1737–1738.
- [36] A. Elkady, F. Abdelmonem, Highly Sensitive and Selective Spectrophotometric Detection of Trace Amounts of Hg 2+ in Environmental and Biological Samples Based on 2,4,7-Triamino-6-Phenylpteridine, 2013.
- [37] D. Karunasagar, J. Arunachalam, S. Gangadharan, *J. Anal. Atomic Spectrom.* 13 (1998) 679–682.
- [38] X.-P. Yan, X.-B. Yin, X.-W. He, Y. Jiang, *Anal. Chem.* 74 (2002) 2162–2166.
- [39] M. Rex, F.E. Hernandez, A.D. Campiglia, *Anal. Chem.* 78 (2006) 445–451.
- [40] J.W. Taraska, W.N. Zagotta, *Neuron* 66 (2010) 170–189.
- [41] M. Feng, P. Zhang, H.-C. Zhou, V.K. Sharma, *Chemosphere* 209 (2018) 783–800.
- [42] C.-X. Yang, H.-B. Ren, X.-P. Yan, *Anal. Chem.* 85 (2013) 7441–7446.
- [43] Y. Zhou, H.-H. Chen, B. Yan, *J. Mater. Chem.* 2 (2014) 13691–13697.
- [44] S. Pramanik, C. Zheng, X. Zhang, T.J. Emge, J. Li, *J. Am. Chem. Soc.* 133 (2011) 4153–4155.
- [45] X.-Y. Xu, B. Yan, *ACS Appl. Mater. Interfaces* 7 (2015) 721–729.
- [46] Q. Tang, S. Liu, Y. Liu, J. Miao, S. Li, L. Zhang, Z. Shi, Z. Zheng, *Inorg. Chem.* 52 (2013) 2799–2801.
- [47] A. Barba-Bon, A.M. Costero, S. Gil, M. Parra, J. Soto, R. Martínez-Máñez, F. Sancenón, *Chem. Commun.* 48 (2012) 3000–3002.
- [48] M. Hmadeh, A.C. Fahrenbach, S. Basu, A. Trabolsi, D. Benítez, H. Li, A.-M. Albrecht-Gary, M. Elhabiri, J.F. Stoddart, *Chem. Eur. J.* 17 (2011) 6076–6087.